Unraveling gas evolution in sodium batteries by online electrochemical mass spectrometry

Mariyappan Sathiya, Leiting Zhang, Chrysi Tsolakidou, Jean-Marie Tarascon, Sigita Trabesinger

Unraveling Gas Evolution in Sodium Batteries by Online Electrochemical Mass Spectrometry

Leiting Zhang[a*1], Chrysi Tsolakidou[a], Sathiya Mariyappan[b,c], Jean-Marie Tarascon[b,c], Sigita Trabesinger[a*]

[a]Battery Electrodes and Cells, Electrochemistry Laboratory, Paul Scherrer Institute, Forschungsstrasse 111, 5232 Villigen-PSI, Switzerland

[b]Chimie du Solide et de l'Énergie, UMR 8260, Collège de France, 11 place Marcelin Berthelot, 75005 Paris, France

[c]Réseau sur le Stockage Electrochimique de l'Énergie (RS2E), Amiens, France

*leiting.zhang@psi.ch, sigita.trabesinger@psi.ch

[1]Present address: Department of Chemistry - Ångström Laboratory, Uppsala University, Box 538, SE-751 21, Uppsala, Sweden. Email: leiting.zhang@kemi.uu.se

Acknowledgements

L. Z. and S. T. are grateful to the financial support from the Swiss Competence Center for Heat and Electricity Research (SCCER–HaE). C. T. thanks the International Association for the Exchange of Students for Technical Experience (IEASTE) for funding her exchange stay at PSI. L. Z. acknowledges fruitful discussions with Petr Novák and Guochun Yan.

Abstract

Gaseous decomposition products from irreversible side-reactions enable understanding of inner working of rechargeable batteries. Unlike for Li-ion batteries, the knowledge of the gas-evolution processes in Na-ion batteries is limited. Therefore, in this study, we have performed online electrochemical mass spectrometry to understand gassing behaviors of model electrodes and electrolytes in Na-ion cells. Our results show that a less stable solid electrolyte interphase (SEI) layer is developed in Na-ion cells as compared with that in Li-ion cells. Electrolyte reduction on the anode has much larger contribution to the gassing in the Na-ion cells, as soluble species migrate to the cathode and be decomposed there. During cell cycling, linear carbonates do not form an SEI layer on the anode, resulting in continuous electrolyte reduction, while cyclic carbonates form a more stable SEI layer, preventing further decomposition of the electrolyte, similarly to Li-ion system but with much higher severity. Besides the standard electrolyte solvents, we have also assessed effects of several common electrolyte additives in stabilizing the interphases. The results of this study provide understanding and guidelines for developing more durable electrolyte–electrode interphase enabling higher specific energy and improved cycling stability for Na-ion batteries.

1. Introduction

Li-ion batteries (LIBs) are accelerating the global energy transition in electrified transport, with significant further cost reduction and performance advancements projected for the near future. Meanwhile, Na-ion batteries (NIBs) are regaining attention, after their initial exposure back in the 1980s, as a geopolitically independent alternative to its lithium counterpart [1,2]. Among the other advantages, it is worth noting is that Al can be used as the anode current collector instead of heavy, expensive, and less malleable Cu, reducing the overall manufacturing cost. Furthermore, the chemical and electrochemical similarities between lithium and sodium chemistries [3–5] facilitate rapid knowledge transfer, such as utilization of layered and polyanion-type cathodes, carbonaceous anodes, alkyl-carbonate–based solvents, and electrolyte additives.

However, not all lessons learned from LIBs can be transferred to NIBs, especially the knowledge concerning metallic anode, as sodium is more reactive, in addition to the fact that metallic Li issues are not yet solved. Such a difference is believed to originate from the chemical stability of the solid electrolyte interphase (SEI), where a higher solubility of Na-based SEI components results in a less durable SEI, and hence, in a higher extent of electrolyte degradation [6–10]. To properly address the interfacial stability issues, apart from scrutinizing physicochemical and electrochemical properties of electrolyte species, including their degradation products [11–14], and looking into the surface chemistry of electrode materials, analyzing gaseous species released from common side-reactions adds one more knowledge block for understanding the interfacial degradation mechanism [15,16]:

$$H_2O/ROH + e^- \rightarrow OH^-/RO^- + 1/2\,H_2\uparrow \quad (1)$$

$$C_3H_4O_3 + Na^+ + e^- \rightarrow 1/2(CH_2OCOONa)_2 + 1/2C_2H_4\uparrow \quad (2)$$

$$C_3H_4O_3 + H_2O/OH^- \rightarrow C_2H_5O_2{}^- + CO_2\uparrow \quad (3)$$

$$Na_2CO_3 + 2H^+ \rightarrow H_2O + 2Na^+ + CO_2\uparrow \quad (4)$$

$$NaPF_6 + H_2O \rightarrow NaF + 2HF + POF_3\uparrow \quad (5)$$

Online electrochemical mass spectrometry (OEMS) has been proven an effective operando technique to quantitatively monitor degradation reactions of LIBs [17–19]. It allows automatic sampling of volatile species from the overhead space of the cell by a quadrupole mass spectrometer through an integrated gas-sampling interface. However, there have been only limited studies on gassing of some specific Na-based systems [20–23], the hypothesis of which have not been verified in other types of NIBs. Therefore, we embarked on a systematic study of the gas evolution in NIBs, using model electrodes and electrolytes, by aiming to provide a comprehensive understanding on the complex interfacial behavior in NIBs from a gas evolution perspective. The paper is structured to stepwise answer the following questions:

- Which gas is formed on Na anode during open circuit?
- What is the individual contribution of linear and cyclic carbonates to gassing?
- What is the contribution of metallic Na anode upon cycling?
- Will electrolyte additives mitigate or increase the extent of cell gassing?
- Will layered cathodes promote more gas release than polyanion-type cathodes?

2. Material and Methods

Electrode materials: Polyanion $Na_3V_2(PO_4)_2F_3$ (NVPF) and $Na_3V_2(PO_4)_3$ (NVP), layered $NaNi_{0.45}Zn_{0.05}Mn_{0.4}Ti_{0.1}O_2$ (NNZMTO) and $NaLi_{1/3}Mn_{2/3}O_2$ (NLMO) were used as cathodes. Hard carbon (HC) and metallic sodium (Na, reagent grade, Sigma Aldrich) were used as anodes. The NVPF, NNZMTO, and NLMO were synthesized according to previous publications [23–25].

Preparation of electrolytes: Battery-grade diethyl carbonate (DEC), dimethyl carbonate (DMC), ethylene carbonate (EC), and propylene carbonate (PC) from BASF were used as electrolyte solvents. All solvents were dried by molecular sieves, prior to being examined by Karl Fischer coulometric titrator (Metrohm AG, Switzerland) showing residual water content lower than 10 ppm. Electrolytes were prepared by dissolving $NaPF_6$ (battery grade, Stella, Japan) into respective solvents to form 1.5 mol L^{-1} and 1 mol L^{-1} of single-solvent and binary-solvent solutions, respectively. Electrolyte additives, such as fluoroethylene carbonate (FEC, > 99.9%, Solvay), vinylene carbonate (VC, 97%, Sigma Aldrich), tris(trimethylsilyl)phosphite (TMSPi, 96%, Alfa Aesar), sodium difluoro(oxalato)borate (NaODFB) were respectively added to a 1 mol L^{-1} of $NaPF_6$ in EC/DMC (1:1 by volume, denoted as NP30) electrolyte. The NaODFB salt was synthesized according to a previous paper [26].

Preparation of electrodes: A slurry comprising 90 wt% of cathode active material, 5 wt% of conductive carbon SuperC65 (Imerys Graphite & Carbon, Switzerland), and 5 wt% of polyvinylidene fluoride binder (PVDF, Solef 5130, Solvay) was cast on Al mesh with a wet thickness of 200 µm and then punched into 15 mm disks. HC anodes were prepared in a similar way, with 8:1:1 weight ratio (HC/SC65/PVDF), a wet thickness of 100 µm, and a punched diameter of 13 mm. All cast electrodes were dried at 120 °C overnight under vacuum, before being transferred into a glovebox. Metallic Na was punched into round disks of 20 mm in diameter.

OEMS experiments: In-house designed OEMS cells were prepared employing various electrode combinations and a piece of Whatman GF/D glassfiber separator (22 mm in diameter) soaked in 150 µL of electrolyte. Na half- and full-cells were assembled in an argon-filled glovebox with water and oxygen level both lower than 0.1 ppm. At least two cells were assembled for each of the combination to verify the reproducibility of the OEMS measurements. Gases and volatile species were collected from the overhead space of the cell and analyzed by a quadrupole mass spectrometer (Pfeiffer, Switzerland). Typical m/z ratios were recorded to follow evolution of possible gases (H_2: m/z = 2, CH_4: m/z = 16, C_2H_4: m/z = 26, C_2H_6: m/z = 28, O_2: m/z = 32, C_3H_6: m/z = 41, CO_2: m/z = 44, POF_3: m/z = 85, etc.). Note that channels 2, 26, 32, 44 have been calibrated using calibration gases (1000 ppm of H_2, C_2H_4, O_2, and CO_2 in Ar, respectively). The channel corresponding to CO (m/z = 28) is not quantitatively measured, as it overlaps with that of N_2 and other hydrocarbons (C_xH_y).

3. Results and Discussion

3.1. Na metal–induced gas evolution at open circuit

In order to understand electrolyte decomposition on surface of Na metal under conditions mimicking open circuit condition, i.e. chemical reactivity upon exposure to electrolyte, we have performed injection experiments in combination with OEMS. 100 µL of NP30 electrolyte were injected into an OEMS cell [27] containing a piece of sodium metal at the cell-bottom and recorded gas evolution profiles (Figure 1). Signals corresponding to formation of H_2, CO_2, and C_2H_4 gases were detected immediately after injection, where both H_2 and CO_2 gases are visible with an initial overshoot (two upper panels of Figure 1), followed by a gradual decay in gas evolution rate within the experimental timeframe. H_2 is formed as the reduction product of residual H_2O and alcohol impurities (Equation 1), while CO_2 stems most likely from catalytic ring-opening of EC (Equation 3). C_2H_4, a characteristic reduction product of EC according to Equation 2, is produced at a lower rate but has slower decay. Such a corrosion-like contribution cannot be neglected when evaluating gas release of electrode materials in half-cells. Therefore, in order to obtain reliable data without interference of gases coming from metallic Na electrode, there is a need to find a non-gassing counter electrode material that does not react with electrolyte. Otherwise the separation of gases, their evolution rates and quantities cannot be reliably assigned to working electrode under analysis, as there is constant reactivity on metallic Na.

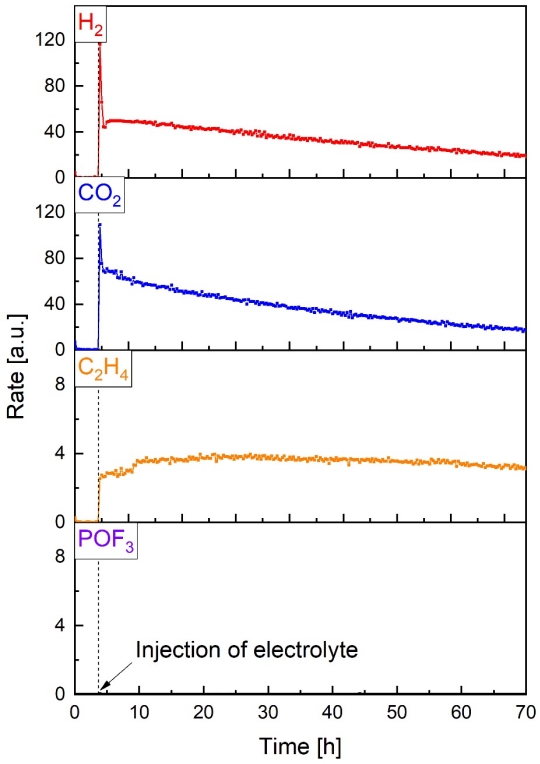

Figure 1 Injection experiment in combination with OEMS, showing continuous gas formation when Na-based electrolyte contacts Na metal.

3.2. Electrolyte solvent effect on gas evolution

As a candidate of non-gassing electrode material, polyanion-type NVP was investigated, knowing that the material is structurally stable and both redox plateaus (ca. 3.4 V for $V^{4+/3+}$ and ca. 1.7 V for $V^{3+/2+}$, Figure S1) should fall within the electrolyte stability window. This also allows us to assemble a NVP || NVP symmetric cell, eliminating possible degradation reactions, which occur when metallic Na is used as the anode. Indeed, no gas release is detected in this cell (Figure 2), confirming that NVP can be used as a non-gassing robust reference electrode with suitable operating potential for NIBs.

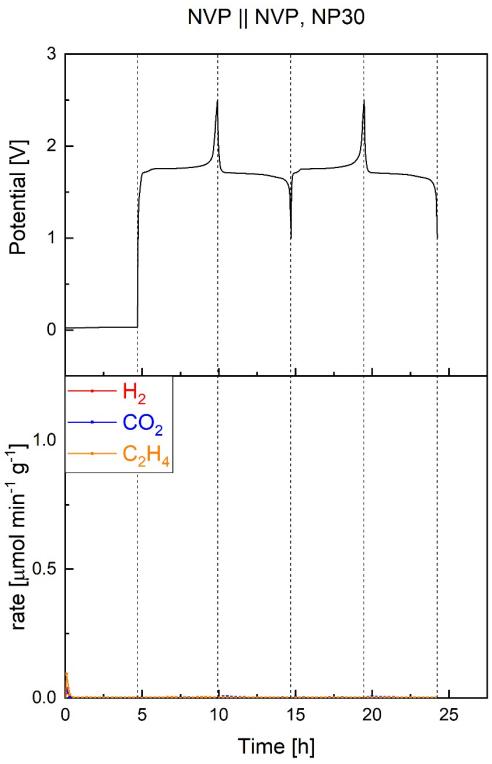

Figure 2 No gas evolution detected from a symmetric NVP || NVP full cell with NP30 electrolyte.

$$C_4H_6O_3 + Na^+ + e^- \rightarrow 1/2(CH_2OCOONa)_2CH_2 + 1/2C_3H_6 \uparrow \quad (6)$$

$$CH_3OCOOCH_3 + Na^+ + e^- \rightarrow CH_3OCOONa + {}^{\cdot}CH_3 \rightarrow CH_4 \uparrow \quad (7)$$

$$C_2H_5OCOOC_2H_5 + Na^+ + e^- \rightarrow C_2H_5OCOONa + {}^{\cdot}C_2H_5 \rightarrow C_2H_6 \uparrow \quad (8)$$

To decipher the redox stability of individual solvents, our approach was to use model single-solvent electrolyte systems to perform OEMS experiments. We purposely selected NVPF as a model cathode, since it enables us to look into the electrolyte stability in two potential regions (3.7 V and 4.2 V vs. Na, respectively), while we chose HC as a model anode for its compatibility with carbonate-based solvents. In both cases, the cells were designed as cathode-limited and gas amounts were normalized to the cathode mass.

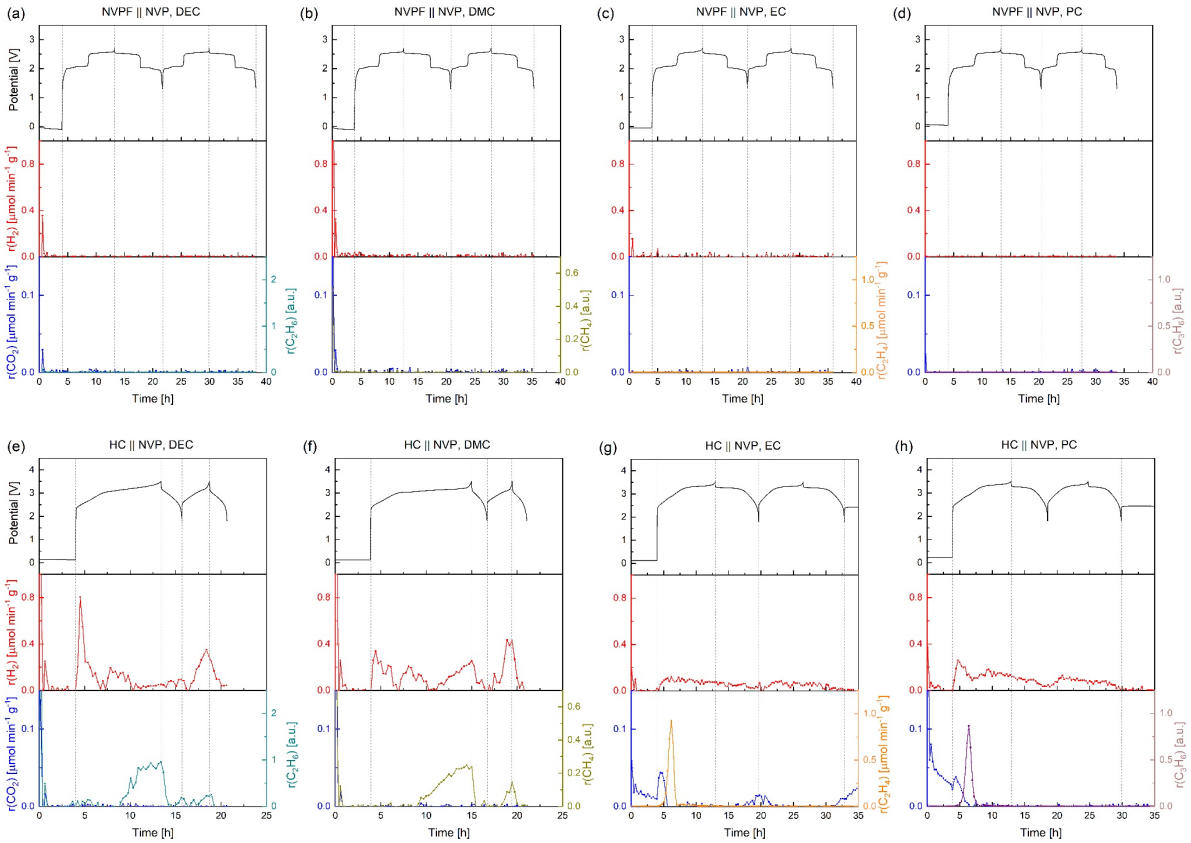

Figure 3 Oxidative stability (a-d) and reductive stability (e-h) of single-solvent electrolytes studied on NVPF || NVP and HC || NVP model systems, respectively. The solvent used is specified on top of individual figures. All gas rates are normalized to the cathode mass.

Figure 3a-d compares the oxidative stability of individual single-solvent electrolytes, as none of the reduction reaction takes place on the side of NVP and only oxidation can occur on NVPF side. Surprisingly, no gas is detected for any of the solvents up to 2.7 V vs. NVP (ca. 4.3 V vs. Na).

Meanwhile, the reductive stability of single-solvent electrolytes (Figure 3e-h) is more complicated, which leads to substantial potential-dependent electrochemically induced gas formation. H_2 formation shows several peaks in both recorded cycles, indicating involvement of multiple reactions, such as reduction of water, alcohol impurities, surface functional groups, and oxidized protic species ($R–H^+$) [28]. C_2H_6 and CH_4 (Figure 3e and f), the reduction products of DEC and DMC [29] (Equation 7 and 8), respectively, forms in the middle of the second H_2 evolution peak (ca. 3.1 V vs. HC), and overlaps with the third one until the end of charge. Whereas the sharp peaks of C_2H_4 and C_3H_6 (Figure 3 g, h), corresponding to EC and PC reduction (Equation 2 and 6), respectively, are emerging between 2.6–3.1 V vs. NVP (ca. 0.8–0.3 V vs. Na). It is also worth noting that trace amount of CO_2 (Figure 3g, h) is formed during OCV for EC and PC, owing to hydrolysis of cyclic carbonates (Equation 3). This reaction quickly ceases when a potential bias is applied, as all of residual water is reduced on the anode.

Overall, both linear carbonate-based (DMC and DEC) electrolytes show poor Coulombic efficiency during the first cycle and an inferior specific capacity as compared to those of the cyclic carbonates (EC and PC). The drastic difference is rooted most likely in the stability of the SEI layer.

3.3. Na metal–induced gas evolution upon cycling

Having examined the reactivity of metallic Na in open circuit and the individual contribution of solvents on gassing of NIBs, we re-assessed gas evolution upon cycling in Na half-cells. Figure 4a-c compares gassing behavior of EC-based single-solvent electrolyte having NVP, NVPF, and HC as working electrodes, respectively, and metallic Na as counter electrode. We also show gassing profiles of an NVPF || HC full-cell (Figure 4d) using the same electrolyte for comparison. All gassing results are normalized to the cathode mass.

In the H_2 evolution profile, spontaneous H_2 release during OCV is observed in all half-cells (Figure 4a-c) but not in the full-cell (Figure 4d). Afterwards, continuous H_2 release is spotted in cells that have either NVP or NVPF working electrode (Figure 4a, b, d) but not in the HC || Na cell (Figure 4c), where H_2 only evolves during OCV and ceases at ca. 0.3 V vs. Na upon first sodiation. We believe that the initial H_2 release is caused by reduction of residual H_2O on the Na anode, as the OCV of 0 V in the full-cell (Figure 4d) does not trigger any spontaneous reduction, hence the absence of H_2 release. Moreover, since all the cells were cycled using the same electrolyte, differences in water content can be excluded. We also eliminate the possibility that continuous H_2 formation in the NVPF || HC (Figure 4d) full cell is solely due to reduction of surface groups of HC, as otherwise we should have observed similar H_2 gassing behavior in the HC || Na (Figure 4c) . Instead, the gassing data strongly suggest that oxidation of by-products on the cathode side at intermediate-to-high potentials promotes the formation of soluble protic species ($R–H^+$), according to Metzger and co-workers [28], which are subsequently reduced on the anode. Such a cross-talk does not come as a total surprise [30,31], as both inorganic [9] (e.g. NaF, Na_2CO_3) and organic [32] (e.g. alkoxide, alky carbonate) SEI components are reportedly more soluble in the electrolyte as compared to their Li-counterparts.

Unlike H_2 that forms solely by reduction, presence of H_2O and other Lewis bases (e.g. OH^-) in the electrolyte may trigger catalytic decomposition of EC (Equation 3) [33], resulting in spontaneous CO_2 release during OCV. In agreement, the spontaneous CO_2 release is again observed for all half-cells (Figure 4a-c) during OCV, but the full-cell also releases trace amount of CO_2, mainly before the SEI is formed (Figure 4d). Upon cycling, most of the cells remain low in CO_2 amount, except the NVPF || Na cell, where the CO_2 release perfectly correlates with the higher plateau of NVPF (4.2 V vs. Na^+/Na^0, Figure 4b). In light of the proposed H_2 formation pathway, we further argue that protons formed by oxidation of by-products on the cathode-side are largely accounting for the additional CO_2 release from the NVPF || Na cell following a chemical decomposition approach (Equation 4) [34]. In contrast, CO_2 stemming from direct oxidation of EC is highly unlikely, according to the result of NVPF || NVP cell in Figure 3c [35]. Further electrolyte characterization, such as nuclear magnetic resonance

spectroscopy (NMR) or liquid chromatography–mass spectrometry (LC-MS), would be complementary to confirm our findings and provide more insights into the nature of soluble by-products in the electrolyte, which is, however, outside the scope of this study.

Last but not least, C_2H_4, stemming from EC reduction at ca. 0.5 V vs. Na^+/Na^0 (Equation 2), is mainly observed in HC-based cells (Figure 4c, d). The amount of C_2H_4 is proportional to the electrochemically active surface area of the negative electrode, which results in negligible amounts of C_2H_4 formed in NVP || Na and NVPF || Na cells (Figure 4a-b).

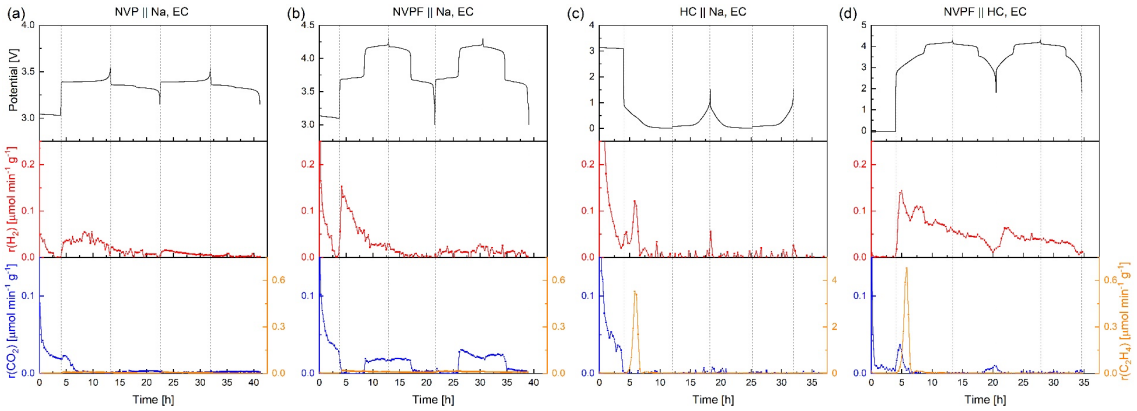

Figure 4 Gassing of EC-based single-solvent electrolyte in (a) NVP || Na, (b) NVPF || Na, (c) HC || Na, and (d) NVPF || HC cells. All gas rates are normalized to the cathode mass.

3.4. Electrolyte-additive–induced gas evolution

Having deciphered gassing contributions using model electrodes and single-solvent electrolytes, we extend our investigation to more "practical" systems, i.e. NVPF || HC full-cells, using standard research-grade electrolytes with various additives, where NP30 serves as the benchmark. The gassing (Figure 5a) of the NVPF || HC full-cell with NP30 as electrolyte highly resembles gas evolution of EC single-solvent electrolyte (Figure 3g), with continuous H_2 formation in both cycles and characteristic C_2H_4 peak during the first charge, demonstrating that EC reduction dominates when using EC–DMC solvent mixture. Trace amount of CO_2 is observed at the end of discharge, which comes most likely from proton-assisted decomposition of carbonates and Lewis-base–assisted ring opening of EC. It is worth mentioning that change of intensity from fragmentation at channel m/z = 16 (CH_4) is not observed, suggesting a more stable SEI layer formed on the HC electrode, preventing DMC reduction at lower potential.

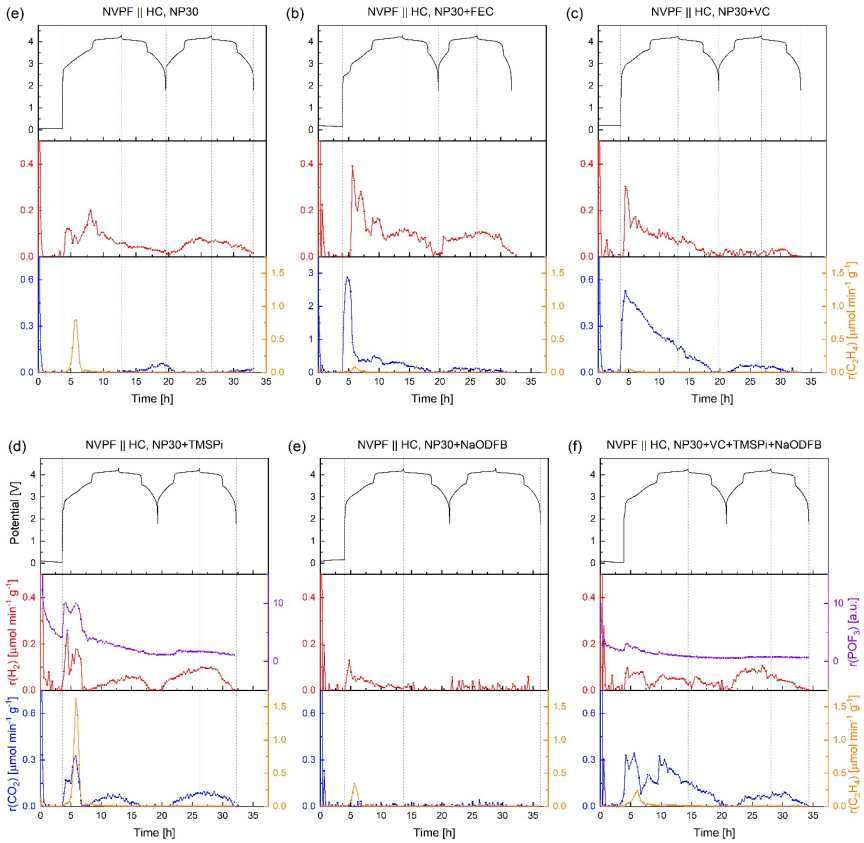

Figure 5 Impact of electrolyte additives on gassing of NVPF || HC full cells. NP30 electrolyte (a) was used as the benchmark. Electrolytes containing (b) 3 wt% FEC, (c) 3 wt% VC , (d) 1 wt% of TMSPi, (e) 0.5 wt% of NaODFB, and (f) mixed VC-TMSPi-NaODFB additives were respectively analyzed. All gas rates are normalized to the cathode mass.

To take one-step further to understand the effects of common electrolyte additives (FEC, VC, TMSPi, and NaODFB), various additive amounts were added to the benchmark NP30 electrolyte. All cells were cathode-limited to avoid Na platting. Gas amounts in Figure 6 and Table S1 are normalized to the cathode mass.

Effect of FEC

FEC has been proven an effective film-forming additive for LIBs, such as for Si and graphite anodes [36–39]. It has a Fermi level lower than the lowest unoccupied molecular orbital (LUMO) of EC, therefore, it is preferentially reduced to form an inorganic-enriched SEI [40].

$$C_3H_3O_3F + Na^+ + e^- \rightarrow \cdot CH_2CHO + NaF + CO_2 \uparrow \qquad (9)$$

With 3 wt% of FEC added to NP30 electrolyte, an additional plateau is observed in Figure 5b at the beginning of charge (ca. 1.2 V vs. Na), accompanied by a significant CO_2 peak, corresponding to roughly half of the total CO_2 release during the first cycle (230.0 out of 443.8 µmol g_{NVPF}^{-1}), followed by much reduced rates until the end of the first cycle. Such behavior is in line with previous studies, proposing stoichiometric reduction of FEC [41]. The different CO_2 evolution rates were interpreted by Jung and co-workers as fast initial formation of a

monolayer SEI, followed by slower growth of subsequent multi-layer, in an Si-based Li-ion cell containing FEC [37]. Consequently, the formation of C_2H_4 as the EC reduction product is mostly suppressed, as can be seen by comparing Figure 5a and 5b. The onset of H_2 formation is right after the main CO_2 peak, indicating that initial FEC reduction does not involve H_2 formation (Equation 9). However, a correlation between CO_2 and H_2 release after the initial CO_2 peak is noted, suggesting H_2 is one of the FEC reduction end-products [37]. It is also supported by a 46% increase of H_2 amount in the first two cycles as compared to the value obtained from the benchmark NP30 electrolyte.

Effect of VC

VC is another widely studied film-forming additive. It undergoes catalytic polymerization upon reduction, forming a poly(VC)-enriched SEI layer [41–44]. In addition, it can also be oxidized on the cathode side, forming a stable cathode electrolyte interphase in LIBs [45–49]. We believe such a beneficial effect can also be extended to NIBs, at least from a gassing perspective. When cycling NVPF || HC full-cell using NP30 electrolyte with 3 wt% of VC (Figure 5c), there is a sharp CO_2 signal upon initial charge, followed by a monotonic decay in CO_2 rate in the first cycle. Consequently, the C_2H_4 evolution is largely mitigated, showing only 10% of the value obtained in the benchmark NP30 electrolyte. Furthermore, a 13% drop of H_2 amount is observed in the first two cycles, as compared to the benchmark, suggesting that the VC-derived interphases are more thoroughly passivating than the solely NP30-derived one, leading to less electrolyte decomposition. Lastly, similar to the FEC-containing electrolyte, there is no sign of DMC reduction in the VC-containing electrolyte.

Effect of TMSPi

TMSPi has been previously proposed to scavenge HF in the electrolyte and prevent transition metal dissolution [50–53]. A notable change, induced by 1 wt% of TMSPi in the NP30 electrolyte, stems from the signal at m/z = 85, corresponding to the formation of POF_3 gas (Figure 5d). In addition, a synchronized evolution of H_2, POF_3, and CO_2 gases is observed at the beginning of charge, while a 90% increase in C_2H_4 amount is noted. Unfortunately, these results did not meet our expectation. For instance, the almost doubled C_2H_4 amount indicates that the SEI layer is poorly formed, most likely owing to unwanted species interfering with the SEI formation process. Furthermore, although the electrolyte is freshly prepared, the quasi-exponential decay of the POF_3 evolution rate strongly suggests spontaneous chemical decomposition of PF_6^- anions, induced by TMSPi. Indeed, such a reaction has been proposed and verified by Qi and co-workers (Equation 10) [54], confirming our assumption. The synchronized gas release, in the meantime, might be caused by reduction of impurities from the commercial TMSPi that we received. To validate this hypothesis, we also tracked channel m/z = 77, corresponding to the formation of Me_3SiF gas (Figure S2), and confirmed the decomposition of TMSPi by HF attack (Equation 11). Therefore, we argue that the purity of the additive is of vital importance to the electrolyte stability and should be carefully controlled.

$$\mathrm{TMSPi} + \mathrm{PF_6^-} \rightarrow \mathrm{TMSPO_xF_y} + \mathrm{POF_3}\uparrow \quad (10)$$

$$\mathrm{TMSPi} + \mathrm{HF} \rightarrow \mathrm{P(OH)(OSiMe_3)_2} + \mathrm{Me_3SiF}\uparrow \quad (11)$$

Effect of NaODFB

The NaODFB and its Li-counterpart (LiODFB) have been proposed as both promising electrolyte salts and additives for rechargeable batteries [55–62]. While some believe that the $ODFB^-$ anion helps passivate the Al current collector [55,58] and form a robust cathode electrolyte interphase (CEI) layer [56,61], others attribute the performance improvement to the formation of a more stable SEI layer on the anode [26,55,59,63]. In an attempt to understand its functionality in NIBs, we cycled NVPF || HC full-cells using NP30 electrolyte with 0.5 wt% of NaODFB (Figure 5e). 59% and 81% drop in C_2H_4 and H_2 formation amounts, respectively, were observed in the first two cycles, while CO_2 and DMC-derived gaseous species were not found. The result signifies a comprehensive protection of the anode from further side-reactions, and confirms that the NaODFB-associated reactions do not release any gas. In addition, there is no sign of NaODFB oxidation, as otherwise CO_2 will be observed as one of the oxidative decomposition products, according to Zhang [55].

Effect of a multi-additive electrolyte

Having reviewed impacts of individual electrolyte additives on modifying the gassing profiles of NVPF || HC cells, we next examined a recently reported promising multi-additive electrolyte for NIBs [26], which consists of 1 mol L^{-1} $NaPF_6$ in EC/DMC (1:1) + 0.5 wt% NaODFB + 1 wt% TMSPi + 3 wt% VC. We expected to find if any synergistic effects can be achieved with respect to gas release, when mixing different additives together. As summarized in Figure 5f and Figure 6, the gassing of the multi-additive electrolyte is not simply the addition of individual contributions. Instead, it shows 55% drop in C_2H_4 amount in the first two cycles, respectively, as compared to the benchmark NP30 electrolyte. From the first glance, this can be attributed to the effect of VC, which strongly suppresses the C_2H_4 release. 20% reduction in H_2 evolution can be ascribed to the role of NaODFB as the additive with the strongest suppression of this gas evolution. In addition, there is no sign of DMC decomposition, as was the case with most of the additives. Instead, additive decomposition products, such as CO_2 and POF_3, can be readily identified, confirming the preferential reduction and decomposition of VC and TMSPi, respectively.

To identify the synergistic effects (if any) among the additives, let's take a closer look at the CO_2 profile (Figure 5f), which shows roughly three stages in the first cycle. In the first stage, namely between OCV and ca. 3.2 V vs. HC, the shape and magnitude of the CO_2 profile highly resembles that of the TMSPi-containing electrolyte (Figure 5d), suggesting the TMSPi may have a higher impact at the beginning of the charge, or simply because its reaction kinetics are faster. The NaODFB salt should also participate in the reduction reactions in the first stage, since we know that it is preferentially reduced before EC to form the SEI layer (Figure 5e). The second stage of CO_2 profile, on the other hand, cannot be immediately assigned to any known process discussed so far. In the third stage, namely between 3.8 and 4.3 V (and also along the first discharge), the CO_2 profile resembles that of the VC-containing electrolyte (Figure 5c), suggesting VC mainly participates in the later stage of the SEI formation cycle. It is clear that the presence of multiple additives alters the decomposition of each other and

modifies the composition of the SEI layer Detailed reaction pathways should be jointly investigated by other characterization techniques, which is beyond the scope of this paper.

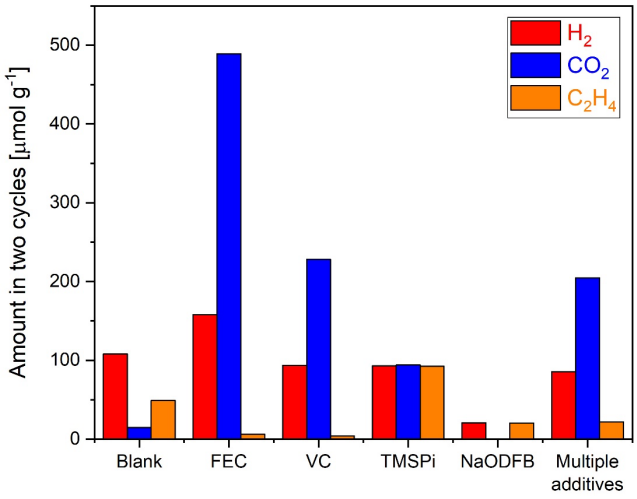

Figure 6 Quantified gas amounts in the first two cycles of NVPF || HC full cells when additives are used in NP30 electrolytes.

3.5. Cathode material–induced gas evolution

We have shown gas evolution of common electrolyte solvents and additives in combination with polyanion-type cathodes NVPF, NVP, and most common HC anode in the model cells. Apart from polyanion cathodes, extensive materials design and investigations are proceeding on layered cathodes [64,65], which also offer outstanding performance over a wide potential range, some of them showing paramount capacities, owing to lattice oxygen redox (known as the anionic-redox). Therefore, we have as well investigated two layered cathodes, namely $NaNi_{0.45}Zn_{0.05}Mn_{0.4}Ti_{0.1}O_2$ (NNZMTO) showing purely cationic redox and $NaLi_{1/3}Mn_{2/3}O_2$ (NLMO) having in addition anionic redox, in an attempt to provide a more comprehensive understanding of gas evolution reactions within NIBs, especially at high potentials (e.g. 4.5 V vs. Na).

We first evaluate the gassing of purely cationic-redox cathodes in NP30 electrolyte. Cells containing layered NNZMTO (Figure 7a-c) were cycled against Na metal, HC, and NVP counter electrodes, respectively. The results are then compared to those having polyanion NVPF as the cathode (Figure 7d-f). It is worth mentioning that, owing to the different voltage–composition profiles of the two materials (solid-solution vs. bi-phasic), the upper cut-off voltage was set to 4.5 V vs. Na^+/Na^0 for NNZMTO, and 4.3 V for NVPF.

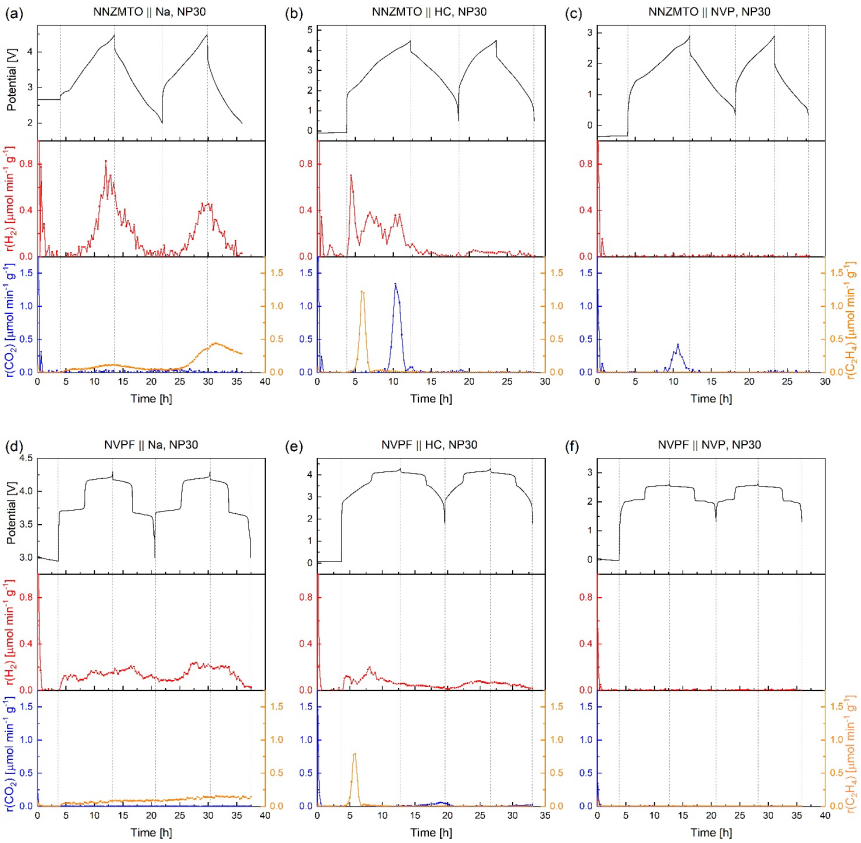

Figure 7 Comparison of gassing profiles between layered NNZMTO (a-c) and polyanion NVPF (d-f), both cycled in NP30 electrolyte against Na, HC, and NVP counter electrodes, respectively. Note that Figure 7e shows the same data as in Figure 5a with updated y-axis scales. All gas rates are normalized to the cathode mass.

NNZMTO || Na vs. NVPF || Na

In the first cycle, the NNZMTO || Na cell (Figure 7a) releases 50% more H_2 than the NVPF || Na cell (Figure 7d). Individually, H_2 evolution onset in the NNZMTO || Na cell (Figure 7a) is as early as ca. 3.4 V, and its rate continues rising until the end of charge, after which the H_2 evolution starts to slow down until reaching potentials below ca. 2.7 V. Similar behavior is also observed in the second cycle, but with a lower rate. In the NVPF || Na cell (Figure 7d), H_2 evolves immediately after the current is applied and an accelerated rate of H_2 evolution is observed on the upper plateau of the NVPF (ca. 4.2 V vs. Na^+/Na^0). As discussed in Section 3.3, the H_2 evolution in both materials should mainly stem from reduction of protons released by oxidative decomposition of by-products at intermediate-to-high potentials. The onset of such an oxidation process is approximated to be 3.4 V vs. Na, which explains why the NVPF || Na cell releases H_2 throughout whole cycling, while in the NNZMTO || Na cell H_2 is only observed after the onset potential is met and stops evolving when the potential is sufficiently low. At present, we cannot completely exclude the possibility that transition metal cations in NNZMTO may catalyze NP30 electrolyte decomposition.

Apart from H_2, we observe a slowly increasing rate of C_2H_4 evolution, while we do not see CO_2 release in cells with both cathodes. At first glimpse, these results may seem contradictory

to the results obtained from the NVPF | EC | Na cell (Figure 4b), where no C_2H_4 is observed and CO_2 evolves at the higher plateau of NVPF. The variation is most likely due to the poor reductive stability of the linear carbonate DMC on metallic Na surface, which we have proven in Figure 4b, where one can see that EC cannot fully passivate the metallic Na anode. Yan and co-workers [32] recently reported that presence of linear carbonates is detrimental to the stability of NIBs, leading to enhanced cross-talk of soluble side-reaction products (e.g. sodium alkoxides and alkyl carbonates) in the cell. Therefore, we believe that DMC should have participated in the SEI formation and altered the composition and hence, the stability of the interphase layer. Therefore, there is a need to review and consider the role of linear carbonates in the conventional Na-based electrolytes, and look for alternatives, possessing low viscosity but with higher resistance to reduction.

NNZMTO || HC vs. NVPF || HC

When HC is used as the counter electrode, a characteristic C_2H_4 peak is noted at the beginning of charge in the first cycle for both NNZMTO- and NVPF-based full-cells (Figure 7b, e), corresponding to the preferential reduction of EC and formation of an SEI layer on the HC surface. No further C_2H_4 evolution is observed, suggesting the SEI layer is more stable than the one formed on metallic Na surface.

Concerning H_2 evolution, the NNZMTO || HC cell releases double amount of H_2 as compared to the NVPF || HC cell. Both full-cells (Figure 7b, e) also release less H_2 compared to their half-cell counterparts, respectively (Figure 7a, d), since HC is better passivated than metallic Na. Furthermore, instead of overlapping H_2 peaks, potential-resolved H_2 evolution processes can be observed in the full-cells. For example, the NNZMTO possesses three H_2 peaks in the first charge and lower rates in the first discharge and the second cycle. The NVPF shows similar trends, except the absence of the third H_2 peak at 3.7–4.3 V vs. HC.

Moreover, there is a distinct CO_2 peak for NNZMTO in the same potential window, which we believe, at least partially, is due to the decomposition of residual Na_2CO_3 on the cathode surface. Surface impurities, such as carbonates and hydroxides, are commonly found for layered oxides in LIBs, where the decomposition mechanism has been extensively discussed [34,66]. We further argue that the CO_2 release is also coupled with the third H_2 peak discussed above, since H_2O may form upon carbonate decomposition (Equation 4), which can be further reduced into H_2 and hydroxide (Equation 1). NVPF on the other hand does not show this peak, since it is less prone to H_2O/CO_2 attack.

NNZMTO || NVP vs. NVPF || NVP

Similar to our previous findings in NVPF || NVP single-solvent cells (Figure 3b, c), neither H_2 nor C_2H_4 is detected in the NNZMTO || NVP cell (Figure 7c) as reduction gaseous products. The only gas we observe is CO_2 from NNZMTO, between 2.2–2.9 V vs. NVP, the same potential window as in the NNZMTO || HC cell. It consolidates our finding that the CO_2 stems from the decomposition of residual carbonates on the surface of NNZMTO. It is also worth mentioning that the amount of CO_2 is less than the one observed in the NNZMTO || HC cell, which is not surprising. As nothing is reduced on the NVP side, there is no dissolved by-

products migrating to and decomposing at the cathode, resulting in less proton formation and diminished CO_2 release.

Moving to an oxygen-evolving system, we briefly comment on gassing of an anionic-redox cathode NLMO based in a previous publication [23]. As illustrated in Figure S3, the presence of singlet $^{\cdot}O$ / molecular O_2 is postulated to mainly account for the drastic oxidation of electrolyte, hence, increasing CO_2 release upon cycling in the NLMO || NVP system, irrespective of solvents used (PC or EC–DEC (1:1)). To verify this hypothesis, NLMO || Na half-cells with PC as the solvent were assembled. While the O_2 and CO_2 release is preserved in the first charge, gassing from the first discharge onward is largely mitigated. Instead, H_2 release is observed during OCV and exists in the following cycles, exactly at the potential window where CO_2 forms in NLMO || NVP cells. Therefore, we conclude that oxygen-evolving cathodes have a detrimental impact on the stability of carbonate-based electrolytes, and that removal of protons from the electrolyte mitigates further carbonate solvent decomposition.

4. Conclusions

In this study, we have presented comprehensive gas-evolution investigation in NIBs, using both model and realistic electrode and electrolyte systems. Owing to the elaborated interfacial reactivity and interfacial compound solubility, the gassing of NIBs is complex. Models established from LIBs may not be always applicable to NIBs. Nevertheless, we offer the experimentally confirmed evidence of many gas-evolution phenomena, occurring within the Na-cells:

- During open circuit voltage, corrosion-like spontaneous electrolyte reduction takes place on Na surface, resulting in H_2, hydrocarbons (C_xH_y), CO_2, etc.
- Both linear and cyclic carbonates do not release gas up to 4.3 V vs. Na, when only oxidative stability is addressed.
- Upon reduction, linear carbonates cannot form a stable SEI layer and will be continuously consumed to form H_2 and alkane (e.g. CH_4, C_2H_6).
- Cyclic carbonates form a more stable SEI layer, where H_2 and alkenes are the main reduction gases. Catalytic ring-opening of cyclic carbonates may take place during OCV, but only with a minimal contribution.
- Cross-talk of soluble species is common in NIBs, often leading to unwanted gas release. For example, H_2 mainly results from reduction of H_2O and impurities in the cell, but protons liberated by oxidation of soluble species will also be reduced to H_2. CO_2 as well has multiple origins, the top two being chemical decomposition of carbonates by protons and catalytic ring-opening of cyclic carbonates by Lewis bases (H_2O/OH^-/CH_3ONa).
- Additives play a decisive role in altering the interfacial behavior of NIBs. FEC and VC help to form a more stable SEI, but extra CO_2 is released as a compromise. NaODFB is able to passivate the anode without introducing gaseous decomposition products,

while TMSPi spontaneously decomposes $NaPF_6$ and its deemed-advantageous role should be re-evaluated.

- The cationic-redox–based layered NNZMTO induces more H_2 and CO_2 release than the polyanion NVPF cathode does. The moisture sensitivity of layered oxides may result in formation of surface impurities, which leads to additional CO_2 release and accelerated electrolyte decomposition in the first cycle.
- Anionic-redox–based layered cathodes release substantial amount of O_2 upon activation, which is extremely detrimental to the stability of carbonate-based electrolyte.

Moreover, to reliably assess performance of Na-ion cells, attention must be paid to the following, often neglected, factors: quality and purity of cell constituents, choice of counter electrode (including high reactivity of Na metal and inertness of NVP electrodes), and to be aware of both gas-releasing and gas-free side-reactions. Frequently, unexpected experimental variations are coming from H_2O introduced by insufficiently dried electrolyte components.

Given the high reactivity of metallic Na, half-cells are often more problematic in terms of side-reactions and gas evolution. Eventually, electrode materials need to be tested in full-cells, especially when cyclability is of high importance. For this, NVP is an excellent reference electrode to study new electrode materials. However, gassing study, based on NVP electrode, may appear too "ideal", as contributions from anode are ignored. Moreover, we want to call to attention that oxidation of reduced electrolyte species may take place as low as 3.4 V vs. Na. Extra cautions needs to be taken when interpreting the gas-evolution results.

In this study, we have demonstrated that operando gas analysis offers a unique approach to studying battery chemistries in real time. However, it is silent to side-reactions that do not involve gas release. Therefore, for deeper understanding of ongoing processes, it must be coupled with other complementary techniques, based on bulk (e.g. transmission electron microscopy), surface (e.g. X-ray photoelectron spectroscopy), and solution (e.g. NMR, LC-MS) phases, to obtain a holistic view of the interfacial behavior.

5. References

[1] J.M. Tarascon, Na-ion versus Li-ion Batteries: Complementarity Rather than Competitiveness, Joule. 4 (2020) 1616–1620. https://doi.org/10.1016/j.joule.2020.06.003.

[2] K. Kubota, S. Komaba, Review—Practical Issues and Future Perspective for Na-Ion Batteries, J. Electrochem. Soc. 162 (2015) A2538–A2550. https://doi.org/10.1149/2.0151514jes.

[3] K.M. Abraham, How Comparable Are Sodium-Ion Batteries to Lithium-Ion Counterparts?, ACS Energy Lett. 5 (2020) 3544–3547. https://doi.org/10.1021/acsenergylett.0c02181.

[4] A. Ponrouch, D. Monti, A. Boschin, B. Steen, P. Johansson, M.R. Palacín, Non-aqueous electrolytes for sodium-ion batteries, J. Mater. Chem. A. 3 (2015) 22–42. https://doi.org/10.1039/c4ta04428b.

[5] A. Ponrouch, M. Rosa Palacín, Post-Li batteries: Promises and challenges, Philos. Trans. R. Soc. A Math. Phys. Eng. Sci. 377 (2019). https://doi.org/10.1098/rsta.2018.0297.

[6] R. Mogensen, D. Brandell, R. Younesi, Solubility of the Solid Electrolyte Interphase (SEI) in Sodium Ion Batteries, ACS Energy Lett. 1 (2016) 1173–1178. https://doi.org/10.1021/acsenergylett.6b00491.

[7] S. Choudhury, S. Wei, Y. Ozhabes, D. Gunceler, M.J. Zachman, Z. Tu, J.H. Shin, P. Nath, A. Agrawal, L.F. Kourkoutis, T.A. Arias, L.A. Archer, Designing solid-liquid interphases for sodium batteries, Nat. Commun. 8 (2017) 898. https://doi.org/10.1038/s41467-017-00742-x.

[8] D.I. Iermakova, R. Dugas, M.R. Palacín, A. Ponrouch, On the Comparative Stability of Li and Na Metal Anode Interfaces in Conventional Alkyl Carbonate Electrolytes, J. Electrochem. Soc. 162 (2015) A7060–A7066. https://doi.org/10.1149/2.0091513jes.

[9] L.A. Ma, A.J. Naylor, L. Nyholm, R. Younesi, Strategies for Mitigating Dissolution of Solid Electrolyte Interphases in Sodium-Ion Batteries, Angew. Chemie Int. Ed. 60 (2021) 4855–4863. https://doi.org/10.1002/anie.202013803.

[10] E. Wang, Y. Niu, Y.X. Yin, Y.G. Guo, Manipulating Electrode/Electrolyte Interphases of Sodium-Ion Batteries: Strategies and Perspectives, ACS Mater. Lett. 3 (2021) 18–41. https://doi.org/10.1021/acsmaterialslett.0c00356.

[11] G. Åvall, J. Mindemark, D. Brandell, P. Johansson, Sodium-Ion Battery Electrolytes: Modeling and Simulations, Adv. Energy Mater. 8 (2018) 1703036. https://doi.org/10.1002/aenm.201703036.

[12] D. Monti, E. Jónsson, A. Boschin, M.R. Palacín, A. Ponrouch, P. Johansson, Towards standard electrolytes for sodium-ion batteries: physical properties, ion solvation and ion-pairing in alkyl carbonate solvents, Phys. Chem. Chem. Phys. 22 (2020) 22768–22777. https://doi.org/10.1039/d0cp03639k.

[13] A. Ponrouch, R. Dedryvère, D. Monti, A.E. Demet, J.M. Ateba Mba, L. Croguennec, C. Masquelier, P. Johansson, M.R. Palacín, Towards high energy density sodium ion batteries through electrolyte optimization, Energy Environ. Sci. 6 (2013) 2361–2369. https://doi.org/10.1039/c3ee41379a.

[14] A. Ponrouch, E. Marchante, M. Courty, J.M. Tarascon, M.R. Palacín, In search of an optimized electrolyte for Na-ion batteries, Energy Environ. Sci. 5 (2012) 8572–8583. https://doi.org/10.1039/c2ee22258b.

[15] B. Rowden, N. Garcia-Araez, A review of gas evolution in lithium ion batteries, Energy Reports. 6 (2020) 10–18. https://doi.org/10.1016/j.egyr.2020.02.022.

[16] S.S. Zhang, Insight into the Gassing Problem of Li-ion Battery, Front. Energy Res. 2 (2014). https://doi.org/10.3389/fenrg.2014.00059.

[17] B. Michalak, B.B. Berkes, H. Sommer, T. Bergfeldt, T. Brezesinski, J. Janek, Gas Evolution in $LiNi_{0.5}Mn_{1.5}O_4$/Graphite Cells Studied In Operando by a Combination of Differential Electrochemical Mass Spectrometry, Neutron Imaging, and Pressure Measurements, Anal. Chem. 88 (2016) 2877–2883. https://doi.org/10.1021/acs.analchem.5b04696.

[18] R. Bernhard, S. Meini, H.A. Gasteiger, On-Line Electrochemical Mass Spectrometry Investigations on the Gassing Behavior of $Li_4Ti_5O_{12}$ Electrodes and Its Origins, J. Electrochem. Soc. 161 (2014) A497–A505. https://doi.org/10.1149/2.013404jes.

[19] A. Guéguen, D. Streich, M. He, M. Mendez, F.F. Chesneau, P. Novák, E.J. Berg, Decomposition of $LiPF_6$ in High Energy Lithium-Ion Batteries Studied with Online Electrochemical Mass Spectrometry, J. Electrochem. Soc. 163 (2016) A1095–A1100. https://doi.org/10.1149/2.0981606jes.

[20] X. Chen, X. Shen, B. Li, H.-J. Peng, X.-B. Cheng, B.-Q. Li, X.-Q. Zhang, J.-Q. Huang, Q. Zhang, Ion-Solvent Complexes Promote Gas Evolution from Electrolytes on a Sodium Metal Anode, Angew. Chemie Int. Ed. 57 (2018) 734–737. https://doi.org/10.1002/anie.201711552.

[21] M. Goktas, C. Bolli, E.J. Berg, P. Novák, K. Pollok, F. Langenhorst, M. v. Roeder, O. Lenchuk, D. Mollenhauer, P. Adelhelm, Graphite as Cointercalation Electrode for Sodium-Ion Batteries: Electrode Dynamics and the Missing Solid Electrolyte Interphase (SEI), Adv. Energy Mater. 8 (2018) 1702724. https://doi.org/10.1002/aenm.201702724.

[22] W. Liu, X. Chen, C. Zhang, H. Xu, X. Sun, Y. Zheng, Y. Yu, S. Li, Y. Huang, J. Li, Gassing in Sn-Anode Sodium-Ion Batteries and Its Remedy by Metallurgically Prealloying Na, ACS Appl. Mater. Interfaces. 11 (2019) 23207–23212. https://doi.org/10.1021/acsami.9b05005.

[23] Q. Wang, S. Mariyappan, G. Rousse, A. V. Morozov, B. Porcheron, R. Dedryvère, J. Wu, W. Yang, L. Zhang, M. Chakir, M. Avdeev, M. Deschamps, Y.S. Yu, J. Cabana, M.L. Doublet, A.M. Abakumov, J.M. Tarascon, Unlocking anionic redox activity in O3-type sodium 3d layered oxides via Li substitution, Nat. Mater. 20 (2021) 353–361. https://doi.org/10.1038/s41563-020-00870-8.

[24] M. Bianchini, N. Brisset, F. Fauth, F. Weill, E. Elkaim, E. Suard, C. Masquelier, L. Croguennec, $Na_3V_2(PO_4)_2F_3$ revisited: A high-resolution diffraction study, Chem. Mater. 26 (2014) 4238–4247. https://doi.org/10.1021/cm501644g.

[25] S. Mariyappan, T. Marchandier, F. Rabuel, A. Iadecola, G. Rousse, A. V. Morozov, A.M. Abakumov, J.M. Tarascon, The Role of Divalent (Zn^{2+}/Mg^{2+}/Cu^{2+}) Substituents in Achieving Full Capacity of Sodium Layered Oxides for Na-Ion Battery Applications, Chem. Mater. 32 (2020) 1657–1666. https://doi.org/10.1021/acs.chemmater.9b05205.

[26] G. Yan, K. Reeves, D. Foix, Z. Li, C. Cometto, S. Mariyappan, M. Salanne, J.M. Tarascon, A New Electrolyte Formulation for Securing High Temperature Cycling and Storage Performances of Na-Ion Batteries, Adv. Energy Mater. 9 (2019) 1–12. https://doi.org/10.1002/aenm.201901431.

[27] C. Bolli, A. Guéguen, M.A. Mendez, E.J. Berg, M.A. Mendez, E.J. Berg, Operando Monitoring of F^- Formation in Lithium Ion Batteries, Chem. Mater. 31 (2019) 1258–1267. https://doi.org/10.1021/acs.chemmater.8b03810.

[28] M. Metzger, B. Strehle, S. Solchenbach, H.A. Gasteiger, Origin of H_2 Evolution in LIBs: H_2O Reduction vs. Electrolyte Oxidation, J. Electrochem. Soc. 163 (2016) A798–A809. https://doi.org/10.1149/2.1151605jes.

[29] D.M. Seo, D. Chalasani, B.S. Parimalam, R. Kadam, M. Nie, B.L. Lucht, Reduction reactions of carbonate solvents for lithium ion batteries, ECS Electrochem. Lett. 3 (2014) 91–94. https://doi.org/10.1149/2.0021409eel.

[30] O.C. Harris, S.E. Lee, C. Lees, M. Tang, Review: mechanisms and consequences of chemical cross-talk in advanced Li-ion batteries, J. Phys. Energy. 2 (2020) 032002. https://doi.org/10.1088/2515-7655/ab8b68.

[31] C. Bommier, X. Ji, Electrolytes, SEI Formation, and Binders: A Review of Nonelectrode Factors for Sodium-Ion Battery Anodes, Small. 14 (2018) 1703576. https://doi.org/10.1002/smll.201703576.

[32] G. Yan, D. Alves-Dalla-Corte, W. Yin, N. Madern, G. Gachot, J.-M. Tarascon, Assessment of the Electrochemical Stability of Carbonate-Based Electrolytes in Na-Ion Batteries, J. Electrochem. Soc. 165 (2018) A1222–A1230. https://doi.org/10.1149/2.0311807jes.

[33] M. Metzger, B. Strehle, S. Solchenbach, H.A. Gasteiger, Hydrolysis of Ethylene Carbonate with Water and Hydroxide under Battery Operating Conditions, J. Electrochem. Soc. 163 (2016) A1219–A1225. https://doi.org/10.1149/2.0411607jes.

[34] A.T.S. Freiberg, J. Sicklinger, S. Solchenbach, H.A. Gasteiger, Li_2CO_3 decomposition in Li-ion batteries induced by the electrochemical oxidation of the electrolyte and of electrolyte impurities, Electrochim. Acta. 346 (2020) 136271. https://doi.org/10.1016/j.electacta.2020.136271.

[35] E. Castel, E.J. Berg, M. El Kazzi, P. Novák, C. Villevieille, Differential Electrochemical Mass Spectrometry Study of the Interface of $x Li_2MnO_3 \cdot (1-x) LiMO_2$ (M = Ni, Co, and Mn) Material as a Positive Electrode in Li-Ion Batteries, Chem. Mater. 26 (2014) 5051–5057. https://doi.org/10.1021/cm502201z.

[36] Y. Horowitz, H.L. Han, F.A. Soto, W.T. Ralston, P.B. Balbuena, G.A. Somorjai, Fluoroethylene Carbonate as a Directing Agent in Amorphous Silicon Anodes: Electrolyte Interface Structure Probed by Sum Frequency Vibrational Spectroscopy and Ab Initio Molecular Dynamics, Nano Lett. 18 (2018) 1145–1151. https://doi.org/10.1021/acs.nanolett.7b04688.

[37] R. Jung, M. Metzger, D. Haering, S. Solchenbach, C. Marino, N. Tsiouvaras, C. Stinner, H.A. Gasteiger, Consumption of Fluoroethylene Carbonate (FEC) on Si-C Composite Electrodes for Li-Ion Batteries, J. Electrochem. Soc. 163 (2016) A1705–A1716. https://doi.org/10.1149/2.0951608jes.

[38] A. Schiele, B. Breitung, T. Hatsukade, B.B. Berkes, P. Hartmann, J. Janek, T. Brezesinski, The Critical Role of Fluoroethylene Carbonate in the Gassing of Silicon

Anodes for Lithium-Ion Batteries, ACS Energy Lett. 2 (2017) 2228–2233. https://doi.org/10.1021/acsenergylett.7b00619.

[39] Y. Jin, N.-J.H. Kneusels, L.E. Marbella, E. Castillo-Martínez, P.C. M M Magusin, R.S. Weatherup, E. Jo, T. Liu, S. Paul, C.P. Grey, Understanding Fluoroethylene Carbonate and Vinylene Carbonate Based Electrolytes for Si Anodes in Lithium Ion Batteries with NMR Spectroscopy, J. Am. Chem. Soc. 6 (2018) 23. https://doi.org/10.1021/jacs.8b03408.

[40] S. Komaba, T. Ishikawa, N. Yabuuchi, W. Murata, A. Ito, Y. Ohsawa, Fluorinated ethylene carbonate as electrolyte additive for rechargeable Na batteries, ACS Appl. Mater. Interfaces. 3 (2011) 4165–4168. https://doi.org/10.1021/am200973k.

[41] A.L. Michan, B.S. Parimalam, M. Leskes, R.N. Kerber, T. Yoon, C.P. Grey, B.L. Lucht, Fluoroethylene carbonate and vinylene carbonate reduction: Understanding lithium-ion battery electrolyte additives and solid electrolyte interphase formation, Chem. Mater. 28 (2016) 8149–8159. https://doi.org/10.1021/acs.chemmater.6b02282.

[42] K.U. Schwenke, S. Solchenbach, J. Demeaux, B.L. Lucht, H.A. Gasteiger, The Impact of CO_2 Evolved from VC and FEC during Formation of Graphite Anodes in Lithium-Ion Batteries, J. Electrochem. Soc. 166 (2019) A2035–A2047. https://doi.org/10.1149/2.0821910jes.

[43] S. Kristiina Heiskanen, J. Kim, B.L. Lucht, S.K. Heiskanen, J. Kim, B.L. Lucht, Generation and Evolution of the Solid Electrolyte Interphase of Lithium-Ion Batteries, Joule. 3 (2019) 2322–2333. https://www.sciencedirect.com/science/article/pii/S2542435119304210 (accessed October 15, 2019).

[44] B. Zhang, M. Metzger, S. Solchenbach, M. Payne, S. Meini, H.A. Gasteiger, A. Garsuch, B.L. Lucht, Role of 1,3-propane sultone and vinylene carbonate in solid electrolyte interface formation and gas generation, J. Phys. Chem. C. 119 (2015) 11337–11348. https://doi.org/10.1021/acs.jpcc.5b00072.

[45] D. Pritzl, S. Solchenbach, M. Wetjen, H.A. Gasteiger, Analysis of Vinylene Carbonate (VC) as Additive in Graphite/LiNi0.5Mn1.5O4 Cells, J. Electrochem. Soc. 164 (2017) A2625–A2635. https://doi.org/10.1149/2.1441712jes.

[46] M. Hekmatfar, I. Hasa, R. Eghbal, D. V. Carvalho, A. Moretti, S. Passerini, Effect of Electrolyte Additives on the $LiNi_{0.5}Mn_{0.3}Co_{0.2}O_2$ Surface Film Formation with Lithium and Graphite Negative Electrodes, Adv. Mater. Interfaces. 7 (2020) 1901500. https://doi.org/10.1002/admi.201901500.

[47] Y. Qian, P. Niehoff, M. Börner, M. Grützke, X. Mönnighoff, P. Behrends, S. Nowak, M. Winter, F.M. Schappacher, Influence of electrolyte additives on the cathode electrolyte interphase (CEI) formation on $LiNi_{1/3}Mn_{1/3}Co_{1/3}O_2$ in half cells with Li metal counter electrode, J. Power Sources. 329 (2016) 31–40. https://doi.org/10.1016/j.jpowsour.2016.08.023.

[48] Y.H. Liu, S. Takeda, I. Kaneko, H. Yoshitake, T. Mukai, M. Yanagida, Y. Saito, T. Sakai, Understanding the Improved High-Temperature Cycling Stability of a $LiNi_{0.5}Mn_{0.3}Co_{0.2}O_2$/Graphite Cell with Vinylene Carbonate: A Comprehensive

Analysis Approach Utilizing LC-MS and DART-MS, J. Phys. Chem. C. 122 (2018) 5864–5870. https://doi.org/10.1021/acs.jpcc.7b10391.

[49] L. El Ouatani, R. Dedryvère, C. Siret, P. Biensan, S. Reynaud, P. Iratçabal, D. Gonbeau, The Effect of Vinylene Carbonate Additive on Surface Film Formation on Both Electrodes in Li-Ion Batteries, J. Electrochem. Soc. 156 (2009) A103. https://doi.org/10.1149/1.3029674.

[50] A. Guéguen, C. Bolli, M.A. Mendez, E.J. Berg, Elucidating the Reactivity of Tris(trimethylsilyl)phosphite and Tris(trimethylsilyl)phosphate Additives in Carbonate Electrolytes - A Comparative Online Electrochemical Mass Spectrometry Study, ACS Appl. Energy Mater. 3 (2020) 290–299. https://doi.org/10.1021/acsaem.9b01551.

[51] C. rolyte Additives for Lithium Ion Batteries: Mechanistic Insights into Differences duPeebles, R. Sahore, J.A. Gilbert, J.C. Garcia, A. Tornheim, J. Bareño, H. Iddir, C. Liao, D.P. Abraham, Tris(trimethylsilyl) Phosphite (TMSPi) and Triethyl Phosphite (TEPi) as Electring $LiNi_{0.5}Mn_{0.3}Co_{0.2}O_2$ -Graphite Full Cell Cycling, J. Electrochem. Soc. 164 (2017) A1579–A1586. https://doi.org/10.1149/2.1101707jes.

[52] J.Y. Jang, Y. Lee, Y. Kim, J. Lee, S.M. Lee, K.T. Lee, N.S. Choi, Interfacial architectures based on a binary additive combination for high-performance Sn_4P_3 anodes in sodium-ion batteries, J. Mater. Chem. A. 3 (2015) 8332–8338. https://doi.org/10.1039/c5ta00724k.

[53] Y.M. Song, C.K. Kim, K.E. Kim, S.Y. Hong, N.S. Choi, Exploiting chemically and electrochemically reactive phosphite derivatives for high-voltage spinel $LiNi_{0.5}Mn_{1.5}O_4$ cathodes, J. Power Sources. 302 (2016) 22–30. https://doi.org/10.1016/j.jpowsour.2015.10.043.

[54] X. Qi, L. Tao, H. Hahn, C. Schultz, D.R. Gallus, X. Cao, S. Nowak, S. Röser, J. Li, I. Cekic-Laskovic, B.R. Rad, M. Winter, Lifetime limit of tris(trimethylsilyl) phosphite as electrolyte additive for high voltage lithium ion batteries, RSC Adv. 6 (2016) 38342–38349. https://doi.org/10.1039/c6ra06555d.

[55] S.S. Zhang, An unique lithium salt for the improved electrolyte of Li-ion battery, Electrochem. Commun. 8 (2006) 1423–1428. https://doi.org/10.1016/j.elecom.2006.06.016.

[56] J. Mun, J. Lee, T. Hwang, J. Lee, H. Noh, W. Choi, Lithium difluoro(oxalate)borate for robust passivation of $LiNi_{0.5}Mn_{1.5}O_4$ in lithium-ion batteries, J. Electroanal. Chem. 745 (2015) 8–13. https://doi.org/10.1016/j.jelechem.2015.02.034.

[57] Z. Chen, Y. Qin, J. Liu, K. Amine, Lithium difluoro(oxalato)borate as additive to improve the thermal stability of lithiated graphite, Electrochem. Solid-State Lett. 12 (2009) A69. https://doi.org/10.1149/1.3070581.

[58] G. Yan, X. Li, Z. Wang, H. Guo, W. Peng, Q. Hu, Lithium difluoro(oxalato)borate as an additive to suppress the aluminum corrosion in lithium bis(fluorosulfony)imide-based nonaqueous carbonate electrolyte, J. Solid State Electrochem. 20 (2016) 507–516. https://doi.org/10.1007/s10008-015-3069-3.

[59] Z.L. Brown, B.L. Lucht, Synergistic Performance of Lithium Difluoro(oxalato)borate and Fluoroethylene Carbonate in Carbonate Electrolytes for Lithium Metal Anodes, J. Electrochem. Soc. 166 (2019) A5117–A5121. https://doi.org/10.1149/2.0181903jes.

[60] J. Chen, Z. Huang, C. Wang, S. Porter, B. Wang, W. Lie, H.K. Liu, Sodium-difluoro(oxalato)borate (NaDFOB): A new electrolyte salt for Na-ion batteries, Chem. Commun. 51 (2015) 9809–9812. https://doi.org/10.1039/c5cc02901e.

[61] T. Deng, X. Fan, L. Cao, J. Chen, S. Hou, X. Ji, L. Chen, S. Li, X. Zhou, E. Hu, D. Su, X.Q. Yang, C. Wang, Designing In-Situ-Formed Interphases Enables Highly Reversible Cobalt-Free $LiNiO_2$ Cathode for Li-ion and Li-metal Batteries, Joule. 3 (2019) 2550–2564. https://doi.org/10.1016/j.joule.2019.08.004.

[62] C. Cometto, G. Yan, S. Mariyappan, J.-M. Tarascon, Means of Using Cyclic Voltammetry to Rapidly Design a Stable DMC-Based Electrolyte for Na-Ion Batteries, J. Electrochem. Soc. 166 (2019) A3723–A3730. https://doi.org/10.1149/2.0721915jes.

[63] J. Liu, Z. Chen, S. Busking, K. Amine, Lithium difluoro(oxalato)borate as a functional additive for lithium-ion batteries, Electrochem. Commun. 9 (2007) 475–479. https://doi.org/10.1016/j.elecom.2006.10.022.

[64] X. Bai, M. Sathiya, B. Mendoza-Sánchez, A. Iadecola, J. Vergnet, R. Dedryvère, M. Saubanère, A.M. Abakumov, P. Rozier, J.M. Tarascon, Anionic Redox Activity in a Newly Zn-Doped Sodium Layered Oxide P2-$Na_{2/3}Mn_{1-y}Zn_yO_2$ ($0 < y < 0.23$), Adv. Energy Mater. 8 (2018) 1802379. https://doi.org/10.1002/aenm.201802379.

[65] E. Talaie, S.Y. Kim, N. Chen, L.F. Nazar, Structural Evolution and Redox Processes Involved in the Electrochemical Cycling of P2−$Na_{0.67}[Mn_{0.66}Fe_{0.20}Cu_{0.14}]O_2$, Chem. Mater. 29 (2017) 5. https://doi.org/10.1021/acs.chemmater.7b01146.

[66] J.K. Papp, N. Li, L.A. Kaufman, A.J. Naylor, R. Younesi, W. Tong, B.D. McCloskey, A comparison of high voltage outgassing of $LiCoO_2$, $LiNiO_2$, and Li_2MnO_3 layered Li-ion cathode materials, Electrochim. Acta. 368 (2021) 137505. https://doi.org/10.1016/j.electacta.2020.137505.